Clamping Angle Control PWM Method to Restore Linear Modulation Range of a Voltage Source Inverter

Jae-Goo Kim, *Member, IEEE*, Kyo-Beum Lee, *Senior Member, IEEE*, and Jung-Wook Park, *Senior Member, IEEE*

***Abstract*—This paper proposes the new clamping angle control (CAC) pulse width modulation (PWM) method to restore its maximum linear modulation range of voltage source inverters (VSIs) reduced by the duty ratio limitation in hardware implementation, which makes the VSIs to operate nonlinearly in the high modulation range. The deadtime and the bootstrap gate driver circuit mainly cause this duty ratio limitation in practice. In particular, the bootstrap gate driver circuit is used in many industrial applications by avoiding the additional power supply to apply the gate-source voltage of power switches, and therefore making the VSIs to be small size with the low cost. First, the proposed CACPWM method is theoretically analyzed. Then, it is applied in the high modulation range to overcome the limitation of the duty ratio due to the use of the bootstrap gate driver circuit. Thereafter, its practical effectiveness is verified by both simulation and experimental tests. Also, the resulting harmonic distortions are compared with those by the conventional PWM methods.**

***Index Terms*—Bootstrap gate driver circuit, clamping angle control (CAC), duty ratio, linear modulation range, pulse width modulation (PWM), voltage source inverter (VSI).**

NOMENCLATURE

t_c	Period of carrier waveform.
t_{cc}	Bootstrap capacitor charging time.
t_d	Deadtime.
t_o	Period of fundamental waveform.
V_P	Positive dc-link voltage.
V_N	Negative dc-link voltage.
V_o	Output voltage of an inverter with respect to V_N.
f_c	Frequency of carrier waveform.
f_o	Frequency of fundamental waveform.
I_o	Output current of an inverter.
x	Subscripts, *u*, *v*, *w* for phase-leg assignment.
$d^p_{\max}$	Maximum practical duty ratio except 1.
d^p_{limit}	Unusable range of a practical duty ratio ($d^p_{\text{limit}} = 1 - \text{d}^p_{\max}$).
$d^p_{\min}$	Minimum practical duty ratio except 0.
$d^*_{\max}$	Maximum reference duty ratio in t_o except 1.
D^*_x	Reference duty ratio for the *x* phase.
D^*_{uv}	Line-to-line reference between D^*_u and D^*_v.
D^{*m}_x	Reference duty ratio limited by $d^p_{\max}$ and $d^p_{\min}$, which is calculated from D^*_x.
D^r_x	Regularly sampled reference of the duty ratio.
D^{rm}_x	Reference duty ratio limited by $d^p_{\max}$ and $d^p_{\min}$, which is calculated from D^r_x.
D^{rc}_x	Reference duty ratio calculated for compensation of deadtime effect.
D^a_x	Actual duty ratio for the *x* phase.
θ_o	Phase offset angle of fundamental waveform.
θ_{PN}	Angle width clamped to V_P or V_N.
θ_P	Angle width clamped to V_P.
θ_N	Angle width clamped to V_N.
θ_{cc}	Clamping control angle.
DPWM	Discontinuous PWM.
DPWM0	DPWM with clamping phase shifted by +30° with respect to DPWM1.
DPWM1	DPWM with θ_{PN} of 60° at the peak value of voltage reference.
DPWM2	DPWM with the clamping phase shifted by –30° with respect to DPWM1.
DPWM3	DPWM with θ_{PN} of 30°.
DPWMMIN	DPWM with θ_N of 120°.
DPWMMAX	DPWM with θ_P of 120°.
$m^p_{\max}$	Maximum modulation index without the difference between D^*_x and D^{*m}_x.
$m^p_{\min}$	Minimum modulation index without the difference between D^*_x and D^{*m}_x.
m_f	Carrier-fundamental frequency ratio ($m_f = f_c/f_o$).
M^*	Reference modulation index.
M^a	Actual output modulation index.
FFT	Fast Fourier transform.
PWM	Pulse width modulation.

Manuscript received June 12, 2017; revised December 27, 2017; accepted February 4, 2018. Date of publication February 15, 2018; date of current version September 28, 2018. This work was supported in part by the National Research Foundation of Korea funded by the Korea government under Grant 2016R1E1A1A-02920095 and in part by the Power Generation and Electricity Delivery Core Technology Program of the Korea Institute of Energy Technology Evaluation and Planning funded by the Ministry of Trade, Industry and Energy, Republic of Korea, under Grant 20171220100330. Recommended for publication by Associate Editor Dorin O Neacsu. *(Corresponding author: Jung-Wook Park.)*

J.-G. Kim and J.-W. Park are with the School of Electrical and Electronic Engineering, Yonsei University, Seoul 03722, South Korea (e-mail: jaegoo@yonsei.ac.kr; jungpark@yonsei.ac.kr).

K.-B. Lee is with the Department of Electrical and Computer Engineering, Ajou University, Suwon 16499, South Korea (e-mail: kyl@ajou.ac.kr).

Color versions of one or more of the figures in this paper are available online at http://ieeexplore.ieee.org.

Digital Object Identifier 10.1109/TPEL.2018.2806376

See http://www.ieee.org/publications_standards/publications/rights/index.html for more information.

CACPWM	Clamping angle control PWM.
SPWM	Sinusoidal PWM.
SVPWM	Space vector PWM.
THD	Total harmonic distortion.

I. Introduction

THE voltage source inverters (VSIs) have been being widely used in many industrial applications such as automobiles, consumer electronics, etc. In general, they generate the harmonics at integer multiples and sidebands of carrier frequency in its linear modulation range by the PWM operation [1]. In general, the maximum linear modulation range of VSIs is from 0 to 0.906, which is $\pi/(2\sqrt{3})$ [2], [3].

In addition, there are the subharmonics associated with the fundamental frequency of a system due to the low frequency ratio, beat components, output voltage errors, and duty ratio limitation. Then, they might cause the audible noises and torque ripples while decreasing the efficiency of a system in practice. Note that the above subharmonics are generated when m_f is lower than 20–30 [4], [5]. Also, they might occur by beat components [6], [7]. In this case, the frequency ratio must be at least over 15 up to 20 to remove them [8]. The voltage errors are caused by the deadtime, turn-ON/OFF delay, voltage drop, etc. [9], of which the deadtime is a major factor causing the nonlinearity of VSIs in PWM operation. Some research works [9]–[11] have reported methods to solve the deadtime problem. Note that the deadtime of approximately 1–2 μs is required for low-voltage applications. In contrast, the traction-driving inverter with the large current rating uses the deadtime of 2–8 μs [11], [12].

The limitation of the PWM duty ratio at both very high and very low duty ratios can reduce the linear modulation range, in which the subharmonics are generated by the limitation. The minimum pulse width is required to solve the over-voltage problem caused by the narrow pulse of voltage [2], [13]. Otherwise, the output voltage of the VSI can suddenly increase two times bigger than its nominal dc value [14]. Thus, it must be 2 or 3 times longer than the oscillation time. For example, the minimum pulse width of 1 μs is practically used for a 100 ft cable [13]. The several control algorithms, which compensate for the modulation index, have been reported in [2] and [15]. However, they can generate the large harmonics. In addition, the variable dwell time control has been introduced in [13]. However, this also cannot increase the maximum value of a linear modulation range. Finally, the use of a bootstrap driver circuit can also cause the practical limitation of the duty ratio. It is widely used in the industry because it avoids the additional switching mode power supply (SMPS) to drive the gate of power switches. Therefore, it enables to make the VSIs with the small size and low cost [16], [17]. However, its use reduces the range of the duty ratio by about 10–20% [18]–[20], which makes the operation of VSIs nonlinear in the high modulation range. Hence, the other solutions such as pulse transformer, optical method, and charge pump drive can be applied instead of using the bootstrap driver circuit [21]–[23]. However, they are expensive for their complex circuits in hardware.

This study proposes the new CACPWM method to restore the linear modulation range of VSIs reduced by the use of the bootstrap gate driver circuit. Then, the proposed method is applied in the high modulation range from 0.6 to 0.906, and the sinusoidal PWM (SVPWM) is used in the modulation range below 0.6. A linear compensation method [10] is used for the deadtime compensation. This paper is organized as follows. Section II theoretically analyzes the practical limitation of the linear modulation range. Thereafter, the proposed CACPWM method and its application strategy are described in Section III. Then, both simulation and experimental results to verify the effectiveness of the proposed method are given in Sections IV and V, respectively. Finally, conclusions are given in Section VI.

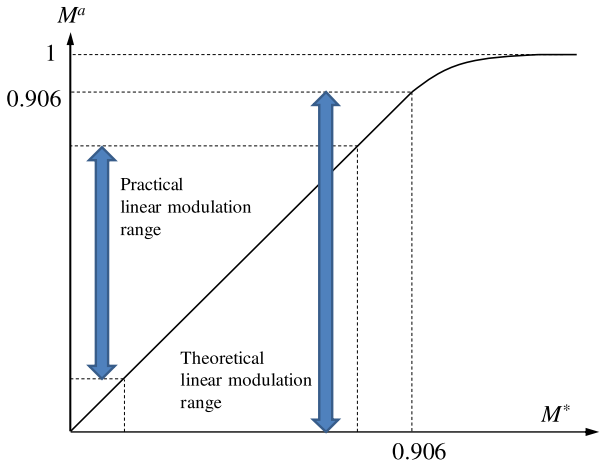

Fig. 1. Practical and theoretical linear modulation ranges of the VSI.

II. Linear Modulation Range in Practice

Fig. 1 shows the variations of M^a for a given M^*. The maximum value of M^a is theoretically 1. However, the maximum value of the linear modulation index is 0.906. In other words, the VSI operates linearly in the range from 0 to 0.906. Moreover, its practical use in hardware implementation can limit this to the smaller range, as shown in Fig. 1. On the other hand, the VSI operates nonlinearly over 0.906. Then, the subharmonics can be generated in this over-modulation (nonlinear) range [24] while causing several problems such as the large amount of harmonic currents, the decrease in the output voltage gain, the abrupt pulse dropping of switching devices, etc. [25]. Even though there are some particular applications used in the over-modulation range, this paper focuses on the operation in the linear modulation range while avoiding the consideration of the above-mentioned subharmonic problems.

The SVPWM and discontinuous PWM (DPWM) methods are widely used for VSI applications. Therefore, their performance will be compared to that of the proposed CACPWM method. Note that the DPWM method includes its six representative methods, which are the DPWM0, DPWM1, DPWM2, DPWM3, DPWMMIN, and DPWMMAX methods.

A. Limitation of the Duty Ratio in Hardware Implementation

Although D^r is ideally in the range from 0 to 1, the ranges of $(0 < D^r < d^p_{\min})$ and $(d^p_{\max} < D^r < 1)$ cannot be used in

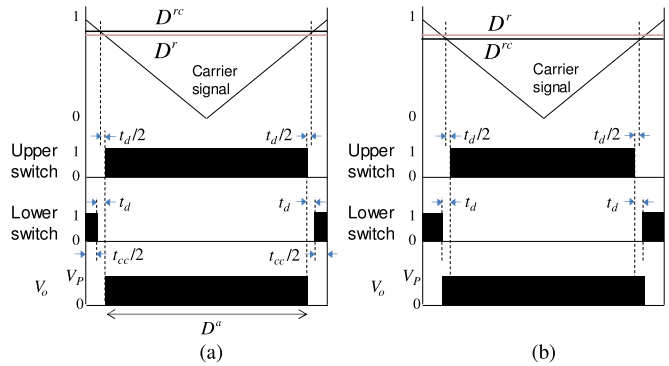

Fig. 2. Switching states when D^r is $d^p_{\max}$. (a) $I_o > 0$. (b) $I_o < 0$.

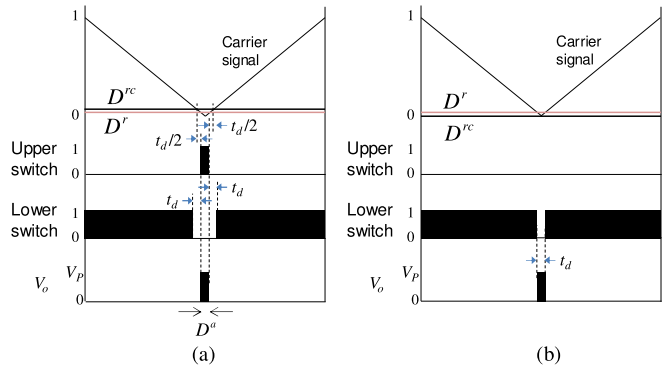

Fig. 3. Switching states when D^r is low. (a) $I_o > 0$. (b) $I_o < 0$.

practice. In the range from $d^p_{\min}$ to $d^p_{\max}$, D^a can be controlled to be the same value of D^r.

In order to define $d^p_{\max}$, the switching state during one switching period is shown in Fig. 2 when D^r is $d^p_{\max}$. When the output current is positive, the output voltage becomes 0 V for t_c, as shown in Fig. 2(a). Then, D^a can be adjusted to the same value of D^r by applying D^{rc} calculated from the compensation algorithm of the deadtime effect. Fig. 2(a) presents the switch state with minimum turn-ON time of the lower switch, which guarantees the time t_{cc}. Otherwise, as shown in Fig. 2(b), when the output current is negative, D^a becomes the same as D^r by applying the compensated reference. Then, d^p_{limit} and $d^p_{\max}$ are expressed as

$$d^p_{\text{limit}} = \frac{t_d + t_{cc}}{t_c} \tag{1}$$

$$d^p_{\max} = 1 - d^p_{\text{limit}}. \tag{2}$$

When D^r is very low, the corresponding switching states are shown in Fig. 3. If the output current is positive, D^a is the same as the turn-ON time of the upper switch, as shown in Fig. 3(a). Then, D^a can be controlled with the same value of D^r until D^r is 0. However, when the output current is negative, D^a can be equal to D^r with the ratio of t_d to t_c, as shown in Fig. 3(b). Thus, D^a can be controlled while t_d is decreased. Therefore, $d^p_{\min}$ becomes zero, and the practical limitation in the low duty ratio is not defined in this case.

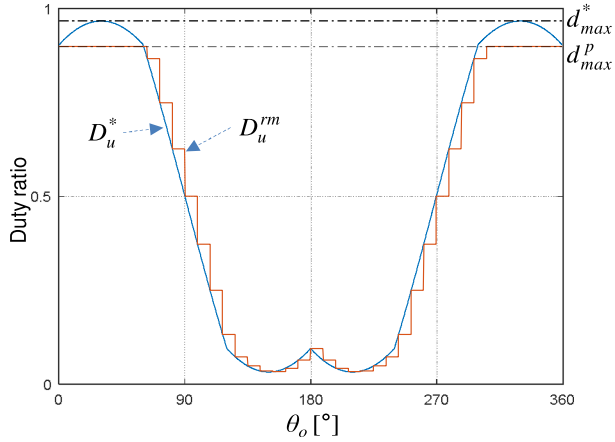

Fig. 4. Limited reference of the duty ratio.

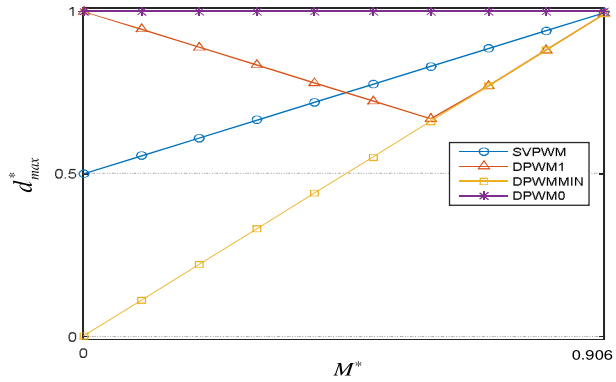

Fig. 5. Comparison of the maximum reference duty ratio ($d^*_{\max}$) by several conventional PWM methods.

B. Reduction of the Linear Modulation Range in Practice

The reference duty ratio of the SVPWM is shown in Fig. 4, where D^{rm}_u is made from D^*_u by the regular sampling with m_f of 40. Then, when it is limited by $d^p_{\max}$, the error by this limitation decreases the linear modulation range. This effect of reduction becomes significant when m_f is large, or $d^p_{\max}$ is small.

The values of $d^*_{\max}$ by four conventional PWM methods, which are the SVPWM, DPWM0, DPWM1, and DPWMMIN methods, are shown in Fig. 5 with three different characteristics for the practical linear modulation range. That is, $d^*_{\max}$ by the SVPWM and DPWMMIN methods increase linearly with respect to M^*. And, when $d^*_{\max}$ is the same as $d^p_{\max}$, the corresponding M^* is $m^p_{\max}$. When the DPWM1 method is used, $d^*_{\max}$ keeps decreasing to M^* of 0.6, and it increases again to the maximum M^* of 0.906. Therefore, there are two values of M^*, which are $m^p_{\max}$ and $m^p_{\min}$, such that $d^*_{\max}$ is the same as $d^p_{\max}$. For the other PWM methods including the DPWM0, DPWM2, DPWM3, DPWMMAX, etc., $d^*_{\max}$ is almost 1 for all M^*. Therefore, these methods may not operate linearly at any M^*. As the result, this paper considers the SVPWM, DPWMMIN, and DPWM1 for the comparison with the proposed CACPWM method.

The maximum modulation index can be calculated from $d^*_{\max}$ because θ_o is fixed for each modulation method when the

reference is $d^*_{\max}$. As shown in Fig. 4, the SVPWM method has $d^*_{\max}$ when θ_o is 30°. Also, the DPWMMIN method has $d^*_{\max}$ when θ_o is 30°. On the other hand, the DPWM1 method has $d^*_{\max}$ at θ_o of 90° when M^* is small, or at θ_o of 30° when M^* is larger than 0.6046. Then, from the definition of the duty ratio in [26], D^*_u of SVPWM and DPWMMIN are expressed, respectively, as follows:

$$D^*_{u(\mathrm{SVPWM})} = 0.5\left(\frac{2\sqrt{3}}{\pi}M^*\cos\left(\theta_o - 30^\circ\right) + 1\right) \quad 0^\circ \le \theta_o \le 60^\circ \tag{3}$$

$$D^*_{u(\mathrm{DPWMMIN})} = -\frac{2\sqrt{3}}{\pi}M^*\cos\left(\theta_o + 150^\circ\right) \quad 0^\circ \le \theta_o \le 120^\circ \tag{4}$$

where the maximum modulation indices of SVPWM and DPWM1 are represented by the following equations if θ_o and D^* are substituted by 30° and $d^p_{\max}$, respectively:

$$m^p_{\max L(\mathrm{SVPWM})} = \frac{\pi}{2\sqrt{3}} \cdot \left(2d^p_{\max} - 1\right) \tag{5}$$

$$m^p_{\max L(\mathrm{DPWMMIN})} = \frac{\pi}{2\sqrt{3}} \cdot d^p_{\max}. \tag{6}$$

For the DPWM1 method, D^*_u is expressed by (7) when θ_o is 30°, and therefore, the maximum modulation index can be given by (6), which is identical to that by the DPWMMIN method. However, when M^* is small, $d^*_{\max}$ of the DPWM1 method is the duty ratio at θ_o of 90°. Then, D^*_u is expressed by (8), and the maximum modulation index can be represented by (9) as follows

$$D^*_{u(\mathrm{DPWM1})} = -\frac{2\sqrt{3}}{\pi}M^*\cos\left(\theta_o + 150^\circ\right) \quad 30^\circ \le \theta_o \le 90^\circ \tag{7}$$

$$D^*_{u(\mathrm{DPWM1})} = 1 + \frac{2\sqrt{3}}{\pi}M^*\cos\left(\theta_o + 30^\circ\right) \quad 90^\circ \le \theta_o \le 150^\circ \tag{8}$$

$$m^p_{\min L(\mathrm{DPWM1})} = \frac{\pi}{\sqrt{3}} \cdot \left(1 - d^p_{\max}\right). \tag{9}$$

In particular, the DPWM1 method has its $m^p_{\max}$ when M^* is greater than 0.6, and it can be computed by (6) for the DPWMMIN. For the SVPWM method, $m^p_{\max(\mathrm{SVPWM})}$ becomes 0.785 if its duty ratio is reduced by 6.7% due to the practical limitation (therefore, $d^p_{\max} = 0.933$). Even though the DPWM1 method has the larger $m^p_{\max}$ than the SVPWM, it still has $m^p_{\min}$. In the conclusion, the DPWMMIN method has the largest linear modulation range among the conventional PWM methods.

III. Proposed CACPWM Method

A. Characteristic of the Proposed CACPWM Method

The proposed CACPWM method operates as a discontinuous modulation method, in which one phase is clamped to V_P or V_N during t_c [27]. However, differently from the conventional DPWM, which uses the fixed θ_P and θ_N of 30°, 60°, or 120° during t_o, the proposed CACPWM method varies θ_P and θ_N according to M^*, as shown in Fig. 6. In other words, θ_P is added by θ_{cc} in the range from 0° to 30°, and θ_N is subtracted by θ_{cc} such that the sum of θ_P and θ_N is always 120° as

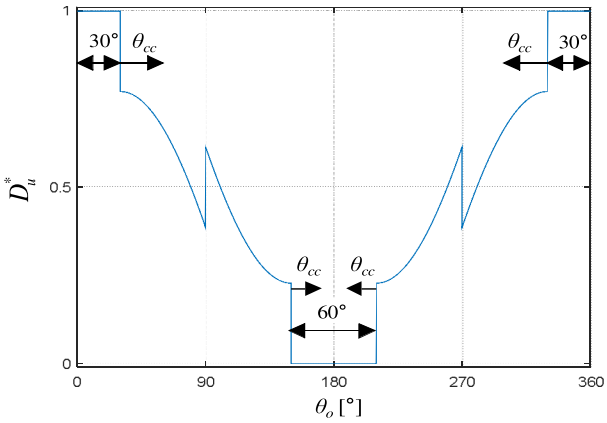

Fig. 6. Waveform of the reference duty ratio (D^*_u) by the proposed CACPWM method.

$$\begin{cases} \theta_P = 60^\circ + 2\theta_{cc} \\ \theta_N = 60^\circ - 2\theta_{cc} \end{cases}. \tag{10}$$

Then, the reference duty ratio of the *u* phase D^*_u of the proposed CACPWM method is controlled as (11). The reference duty ratios for the other *v* and *w* phases D^*_v and D^*_w are controlled by the phase differences of 120° and 240° from D^*_u, respectively. Note that the proposed CACPWM method has the same D^* as the DPWM1 and DPWMMAX methods when θ_{cc} are 0° and 30°, respectively

$$D^*_u = \begin{cases} 1, & 0^\circ \le \theta_o \le 30^\circ + \theta_{cc} \\ M_1\cos\left(\theta_o - 30^\circ\right), & 30^\circ + \theta_{cc} \le \theta_o \le 90^\circ - \theta_{cc} \\ 1 + M_1\cos\left(\theta_o + 30^\circ\right), & 90^\circ - \theta_{cc} \le \theta_o \le 150^\circ + \theta_{cc} \\ 0, & 150^\circ + \theta_{cc} \le \theta_o \le 210^\circ - \theta_{cc} \\ 1 + M_1\cos\left(\theta_o - 30^\circ\right), & 210^\circ - \theta_{cc} \le \theta_o \le 270^\circ + \theta_{cc} \\ M_1\cos\left(\theta_o + 30^\circ\right), & 270^\circ + \theta_{cc} \le \theta_o \le 330^\circ - \theta_{cc} \\ 1, & 330^\circ - \theta_{cc} \le \theta_o \le 360^\circ \end{cases} \tag{11}$$

where $M_1 = \frac{2\sqrt{3}}{\pi}M^*$.

B. Selection of a Clamping Control Angle

To restore the original linear modulation range based on the proposed CACPWM method, θ_{cc} is first selected in offline such that $d^*_{\max}$ is minimized for each M^*, as shown in Fig. 6. Then, they are stored in the look-up table of the hardware memory of the VSI, and they are operated in real-time.

The proposed CACPWM method has $d^*_{\max}$ when θ_o is "30° + θ_{cc}" or "90° − θ_{cc}". Its reference duty ratio can be expressed by

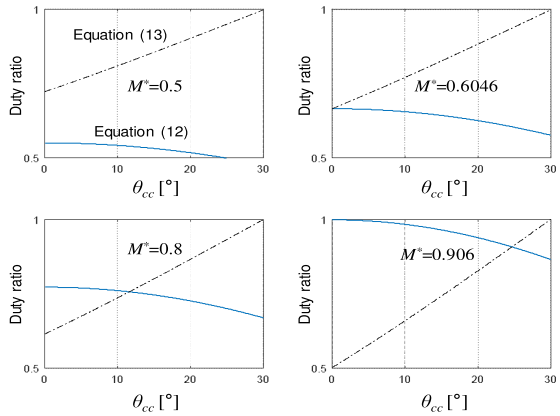

Fig. 7. Variations of D^* in (12) and (13) depending on the values of θ_{cc} when θ_o is $30^\circ + \theta_{cc}$ or $90^\circ - \theta_{cc}$.

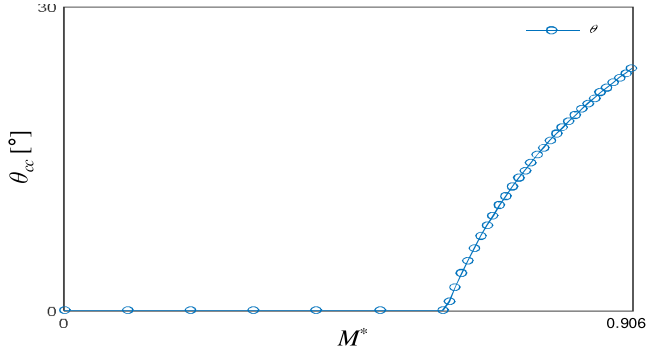

Fig. 8. Selection of θ_{cc} to minimize $d^*_{\max}$ for each M^*.

(12) and (13) based on (11). Then, θ_{cc} for each M^* is calculated such that the larger one among values of the following equations is minimized:

$$D_u^* = M_1 \cos(\theta_{cc}) \tag{12}$$

$$D_u^* = 1 + M_1 \cos(120^\circ - \theta_{cc}). \tag{13}$$

The variations of D^* in (12) and (13) depending on the values of θ_{cc} are shown in Fig. 7. When M^* is small, $d^*_{\max}$ of the CACPWM method is identical to that of the DPWM1 method. However, when M^* is larger than 0.6046, $d^*_{\max}$ of the CACPWM method becomes the point of intersection on the variations by (12) and (13), which is the optimal clamping control angle. It is shown in Fig. 8.

It is observed from Fig. 8 that θ_{cc} is kept to be 0 until M^* becomes 0.6. After that, it is increased to 24.22° at maximum when M^* is 0.906. Therefore, the use of the proposed CACPWM method is the most effective in the ranges with M^* over 0.6 while restoring the linear modulation range of VSIs reduced by the use of the bootstrap gate driver circuit. Otherwise, it will operate as the DPWM1. $d^*_{\max}$ of the proposed CACPWM method is shown in Fig. 9. It is clearly observed that the proposed CACPWM method has the lowest $d^*_{\max}$ among all PWM methods when M^* is over 0.6. In particular, the value of $d^*_{\max}$ corresponding to M^* of 0.906 is 0.9. This means that the proposed CACPWM method can restore the original maximum

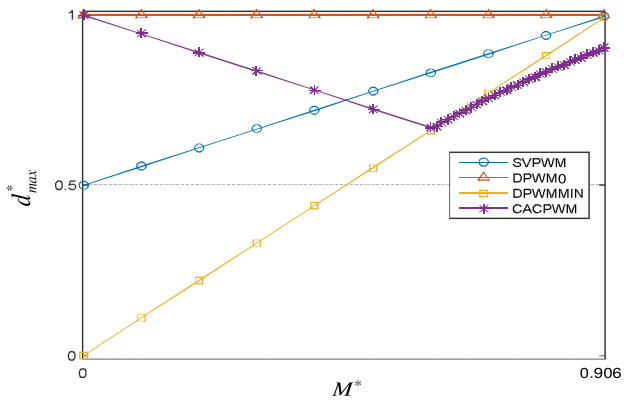

Fig. 9. Maximum reference duty ratio ($d^*_{\max}$) of the proposed CACPWM method.

linear modulation range even though d^p_{limit} is limited by 10% due to the hardware implementation. Moreover, it still provides the larger linear modulation range than the other PWM methods even when d^p_{limit} is limited by more than 10%.

C. PWM Strategy

Because the proposed CACPWM method has the same limitation of the duty ratio as the DPWM1 in the low modulation range, the SVPWM or DPWMMIN method is used together. In general, the SVPWM method provides the better harmonic performance in the range with M^* below 0.6 than the DPWMMIN method [28], [29]. Therefore, for this study, the proposed CACPWM method is applied to the VSI in the range with M^* over 0.6, and the SVPWM method is practically used in the other range.

IV. Simulation Results

The performances of the proposed CACPWM method are first evaluated with the comparison of those of SVPWM, DPWM1, and DPWMMIN methods by simulation test. Note that the other DPWM0, DPWM2, DPWM3, and DPWMMAX methods have distortions of the reference duty ratio when there is the limitation of the duty ratio. When M^* is 0.85 and d^p_{limit} is 0.1, the waveforms of D_u^* and D_{uv}^* are shown in Fig. 10. When D_u^* is lower than the threshold value d^p_{th} defined by (14), the reference becomes $d^p_{\max}$. In contrast, when D_u^* is higher than d^p_{th}, the reference becomes 1 [30]

$$d^p_{\text{th}} = d^p_{\max} + \frac{1}{2}(1 - d^p_{\max}). \tag{14}$$

It is observed that the line-to-line D_{uv}^* in the range from –1 to 1 is two times bigger than the line-to-ground D_u^* in the range from 0 to 1, and it is shifted by +30° for D_u^*. In particular, it is clearly shown that the reference waveform of D_{uv}^* by the SVPWM, DPWM1, and DPWMMIN methods is distorted due to the saturation of D_u^* to $d^p_{\max}$ in the relatively wide range of θ_o when D_u^* is bigger than $d^p_{\max}$. Also, the responses of D_u^* and D_{uv}^* are abruptly changed when the transition of D_u^* occurs between $d^p_{\max}$ and 1. In contrast, the response of D_{uv}^* is

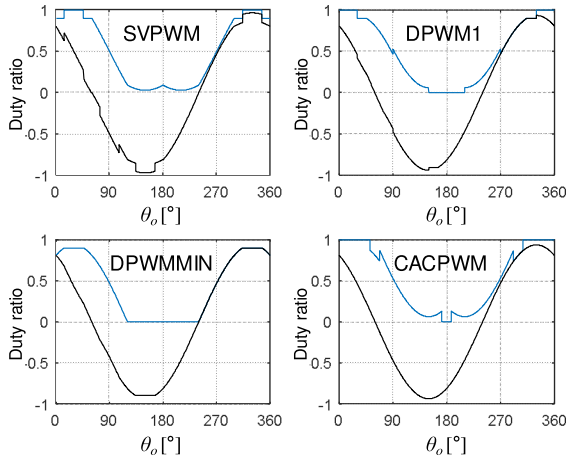

Fig. 10. Simulation results when M^* is 0.85 and d^p_{limit} is 0.1: D^*_u (blue line) and D^*_{uv} (black line).

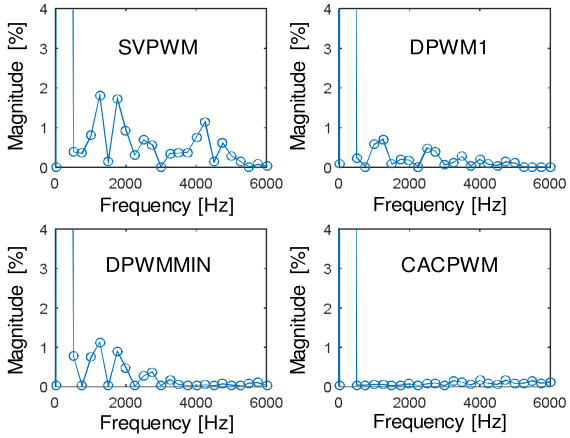

Fig. 11. FFT results of V_{uv} when M^* is 0.85 and d^p_{limit} is 0.1.

not distorted when the proposed CACPWM method with θ_P of 104°, θ_N of 16°, and θ_{cc} of 22° is applied. This is because the CACPWM method does not use D^*_u over 0.9. In other words, $d^*_{\max}$ by the CACPWM method becomes 0.9 when M^* is 0.906.

When the VSI operates with d^p_{limit} of 0.1, f_c of 20 kHz, and f_o of 250 Hz, the FFT results of V_{uv} are shown in Fig. 11. They are regularly sampled from the results of Fig. 10. For the lower order harmonics, the FFT result by the proposed CACPWM method is compared with that by the SVPWM, DPWM1, and DPWMMIN methods. The maximum values for fifth- and seventh-order harmonics are 2%, 0.8%, and 1.2% for the SVPWM, DPWM1, and DPWMMIN methods, respectively. In contrast, it is below 0.1% by the proposed CACPWM method while showing the best harmonic performance.

Also, the weighted-THD (WTHD) of the output voltage is calculated by the following equation, and their values with respect to M^* depending on different m_f and $d^p_{\max}$ are compared in Fig. 12

$$\text{WTHD}_V = \frac{\sqrt{\sum_{n=2}^{\infty}(V_n/n)^2}}{V_1}. \tag{15}$$

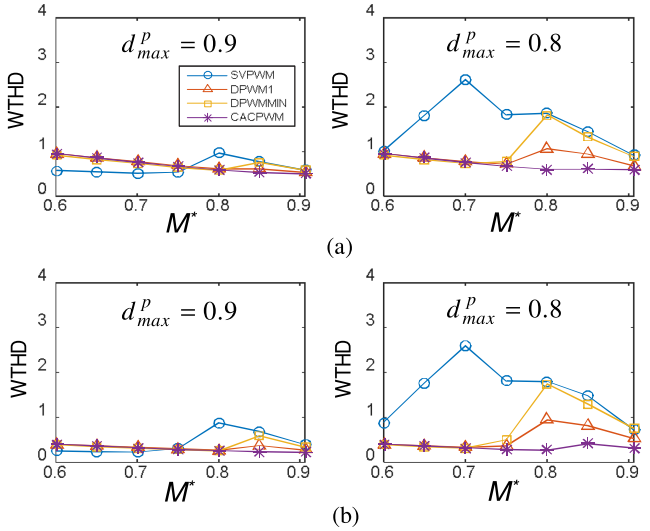

Fig. 12. Comparison of WTHD of V_{uv}: (a) $m_f = 80$ and (b) $m_f = 200$.

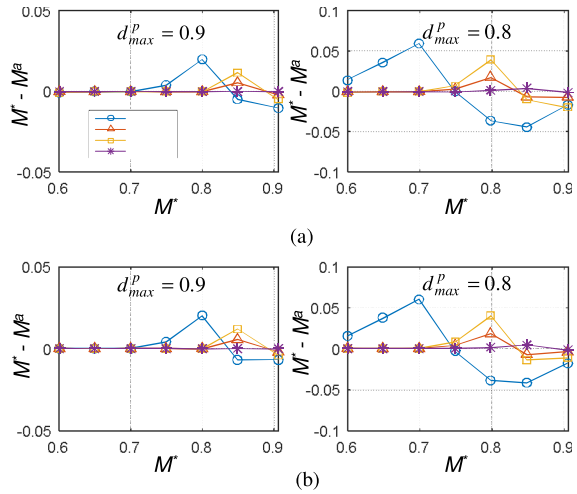

Fig. 13. Difference between M^* and M^a: (a) $m_f = 21$ and (b) $m_f = 200$.

When $d^p_{\max}$ is 0.9, $m^p_{\max}$ are 0.725 for the SVPWM method and 0.816 for both the DPWM1 and DPWMMIN methods. When $d^p_{\max}$ is 0.8, $m^p_{\max}$ are 0.544 for the SVPWM method and 0.725 for both the DPWM1 and DPWMMIN methods. In contrast, $m^p_{\max}$ of the proposed CACPWM method is 0.906, which is the ideal maximum linear modulation index, for both cases. Particularly when $d^p_{\max}$ is small, the proposed CACPWM method shows much better performance than the other PWM methods. Also, the large value of m_f improves the WTHD of the CACPWM method regardless of $d^p_{\max}$. To evaluate the linearity of the modulation index more clearly, the difference between M^* and M^a is calculated, as shown in Fig. 13. It is clearly observed that the proposed CACPWM method provides the best performance among all PWM methods. Note that there m_f has the little effect on the linearity of the modulation index. Each PWM method starts to have the error between M^* and M^a from its $m^p_{\max}$. This is the same as the analysis of WTHD.

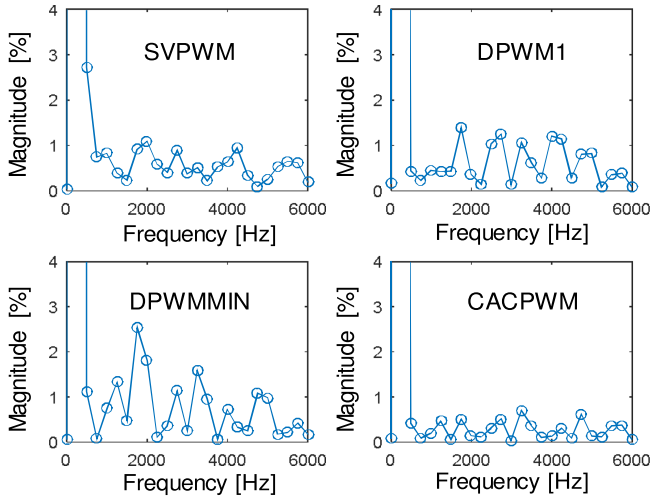

Fig. 14. FFT results of V_{uv} considering deadtime effect when M^* is 0.85 and d^p_{limit} is 0.1.

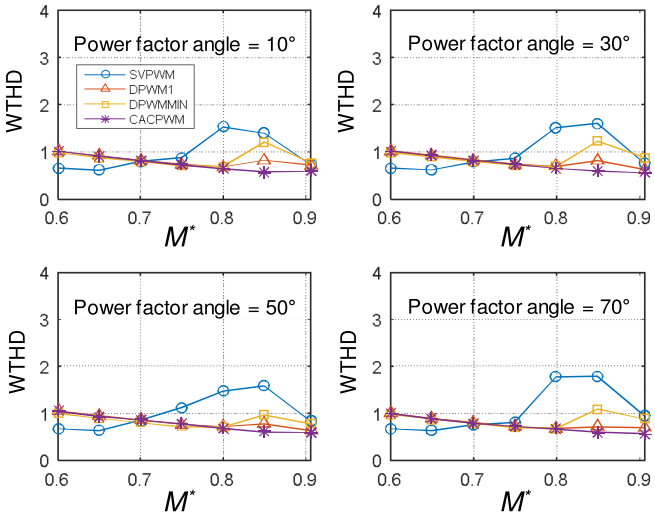

Fig. 15. Comparison of WTHD of V_{uv} depending on different PFs when m_f is 80.

For each method, the error increases, and then it decreases to a negative value because the reference duty ratio at the unused range (from $d^p_{\max}$ to 1) is determined at the midvalue between $d^p_{\max}$ and 1.

The deadtime effect is considered for practical implementations. For the compensation of deadtime effect, a linear compensation method is used in this paper [10]. The simulation results considering the deadtime effect are shown in Fig. 14. The magnitudes of FFT analysis by all PWM methods are increased for most harmonics in low frequency. Nevertheless, the distortions below 0.8% are observed for the proposed CACPWM method, which still shows the best harmonic performance among all PWM methods.

While considering the deadtime effect, the harmonic performance of WTHD and reference linearity depending on different power factors (PFs) are shown in Figs. 15 and 16, respectively. Note that m_f is 80 and $d^p_{\max}$ is 0.9. Both results show the

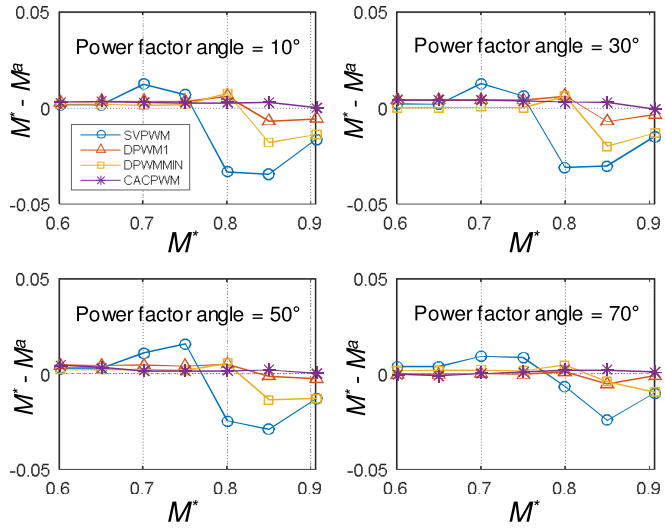

Fig. 16. Difference between M^* and M^a depending on different PFs when m_f is 80.

similar tendency to those in Figs. 12 and 13, and the proposed CACPWM method still shows the better performance than the other three PWM methods.

V. Experimental Verifications

A. Hardware Implementation

The effectiveness of the proposed CACPWM method is verified on the three-phase VSI system of 10 kW applied to the practical mild hybrid vehicle in the industry, as shown in Fig. 17(a).

The practical VSI in Fig. 17(a) uses the bootstrap gate driver circuit and metal–oxide–semiconductor field-effect transistor (MOSFET) switches. Their maximum ratings are the drain-to-source voltage of 80 V and the drain current of 300 A. Also, the total gate charge of MOSFET is 564 nC. The bootstrap capacitor of 2.2 μF is used, and it is designed with the charging time of 8 μs. This practical VSI has the deadtime of 2 μs at the maximum current. Therefore, $d^p_{\max}$ becomes 0.9 when its switching frequency is 20 kHz. The 32-bit microcontroller with the maximum core frequency of 120 MHz is used to implement the proposed method in real-time. Also, the practical induction motor with the rated power of 10 kW is used for the test load, as shown in Fig. 17(b). The oscilloscope of Lecroy WaveSurfer 104Xs-A is used to measure the voltages and currents. That is, the high-voltage differential probe of LeCroy ADP305, which has the bandwidth of 100 MHz, is used for the voltage measurement. Also, the current probe of LeCroy CP500 is used for the current measurement.

B. Experimental Results

The output voltages and currents by the SVPWM, DPWM1, and proposed CACPWM methods are first measured when M^* is 0.85. Their fundamental frequency is adjusted to 250 Hz.

The results are shown in Fig. 18. It is observed from Fig. 18(a) that the VSI by the SVPWM method operates with the proper responses of line-to-line voltage $V_{u\nu}$ and phase current I_u. When

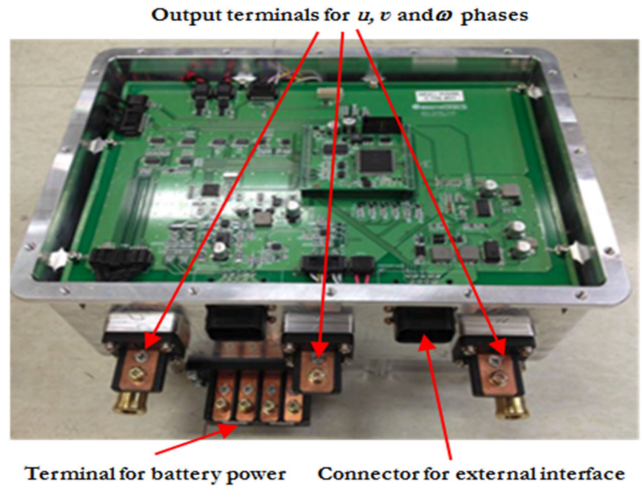

(a)

(b)

Fig. 17. Hardware implementation. (a) VSI of 10 kW. (b) Induction motor test set-up.

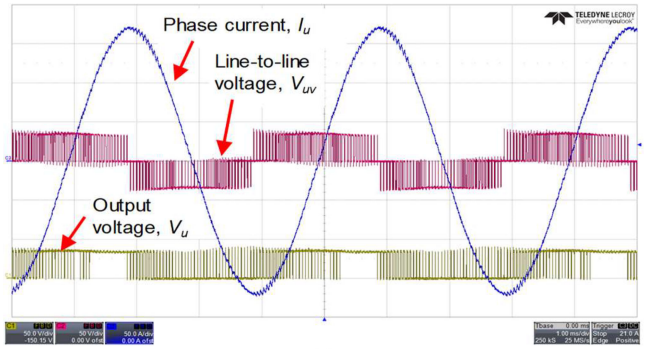

(a)

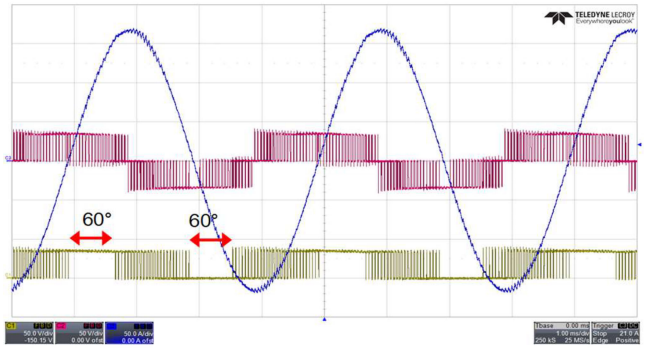

(b)

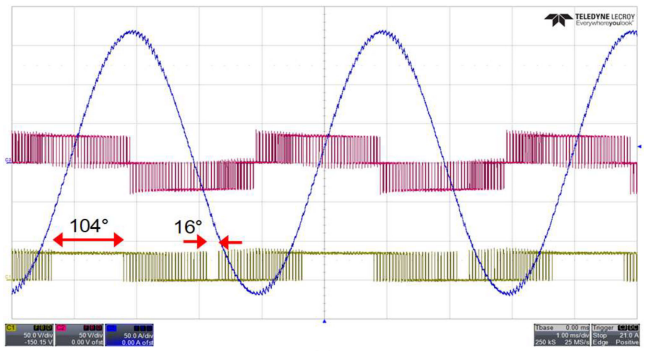

(c)

Fig. 18. Output voltages and currents when M^* is 0.85 and $d^p_{\max}$ is 0.9. (a) SVPWM. (b) DPWM1. (c) CACPWM.

the DPWM1 method is used, the ranges, where V_u is clamped to V_P and V_N, remain constant by 60°, as shown in Fig. 18(b). Finally, when the proposed CACPWM method is applied, M^* is 0.85. Thus, θ_{cc} of 22° is selected in the look-up table formed from Fig. 8. Then, θ_P of 104° and θ_N of 16° are obtained by (10). These calculated values are the same as those of the experimental result in Fig. 18(c).

All output voltages and currents in the experimental test are measured by 25 samples/μs. These measured data during t_o are used for the FFT calculation by using the MATLAB software. In other words, the measured data of 10 000 samples (=25 samples/μs $\times$ 4 ms) and 5000 samples (=25 samples/μs $\times$ 2 ms) are used for the FFT calculation of 250 and 500 Hz waveforms, respectively. Then, the FFT results of the output voltage are shown in Fig. 19. The low-frequency harmonic components of about 1–2% are observed for the SVPWM and DPWM1 methods. However, they are less than 1% by the proposed CACPWM method, which shows the best harmonic performance. This experimental result shows the very good agreement with the simulation result of Fig. 14.

When the induction motor operates in a high current mode, the values of WTHD of V_{uv} with respect to M^* depending on different $d^p_{\max}$ are compared in Fig. 20(a). This result is consistent with the simulation results in Figs. 12 and 15 except for the small difference of about 0.5% due to the practical issues such as voltage drop in the power switches and parameter imbalance of the motor. Also, the values of THD of I_u are compared in Fig. 20(b). The superior performance of the CACPWM method to the other methods becomes obvious particularly when $d^p_{\max}$ is small. In addition, it is observed from the result of Fig. 20(c) that the proposed CACPWM method can restore the linearity of the modulation index up to its maximum value M^* of 0.906 when $d^p_{\max}$ is 0.9. Even when $d^p_{\max}$ is 0.8, which is smaller than 0.9, the CACPWM method still provides the best performance while restoring almost linear modulation range.

The experimental test is also carried out in a low current mode when f_o is 500 Hz and m_f is 40. The PF angle is 55°. Then, the output voltage and current waveforms are shown in Fig. 21. In this low current mode, only harmonic performance

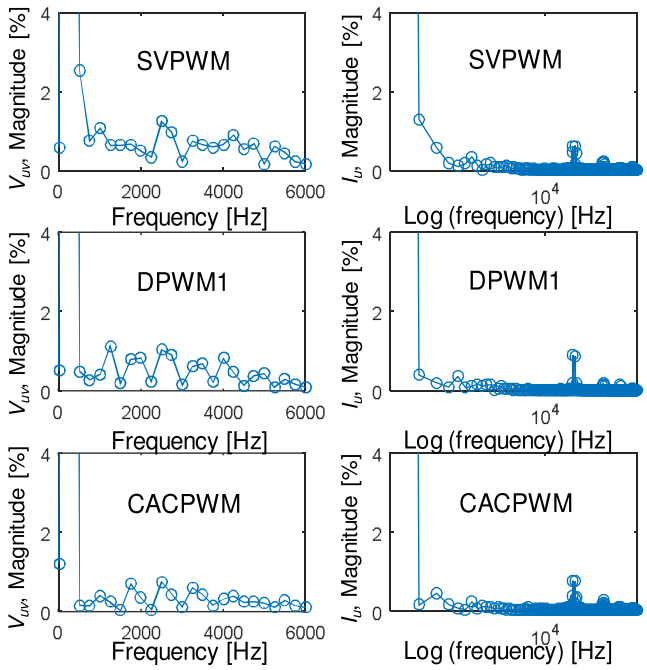

Fig. 19. FFT results for V_{uv} measured from the experimental test.

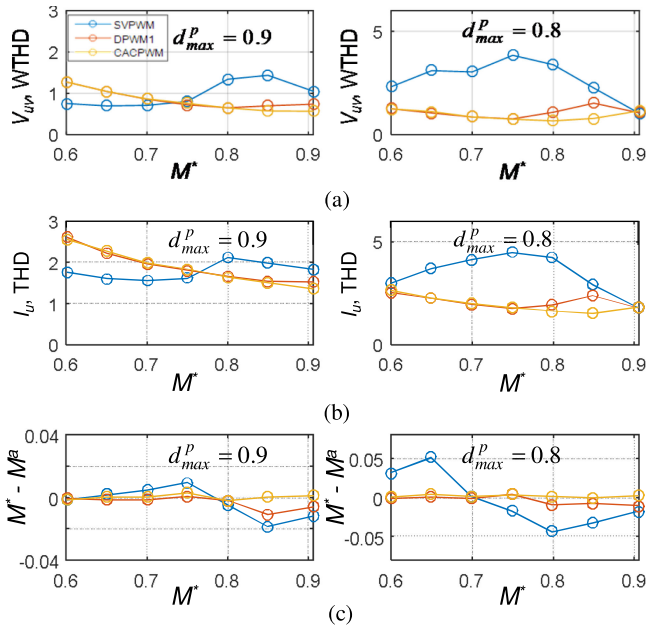

Fig. 20. Experimental results in the high current mode. (a) WTHD of V_{uv}. (b) THD of I_u. (c) difference between M^* and M^a.

is analyzed because the linearity of the modulation index is maintained under the condition, where m_f is higher than 21.

When $d^p_{\max}$ are 0.9 and 0.8, the values of WTHD of V_{uv} are shown in Fig. 22(a). They show a similar tendency to the simulation result in Fig. 15. In particular, the values of WTHD of V_{uv} in this low current mode are increased by about 1% when compared to those in Fig. 20. This is caused by the low m_f. Also, the values of THD of I_u are shown in Fig. 22(b). They

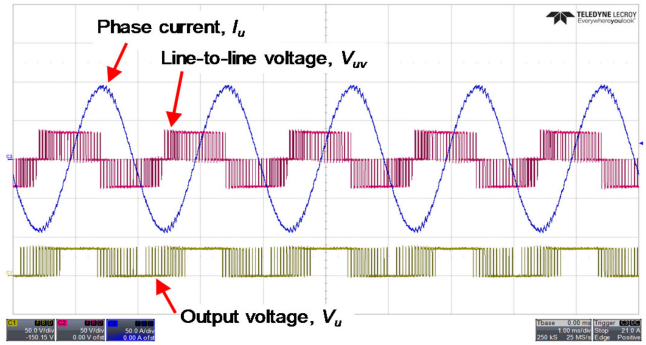

Fig. 21. Output voltage and current by the proposed CACPWM method in the low current mode when M^* is 0.85 and $d^p_{\max}$ is 0.9.

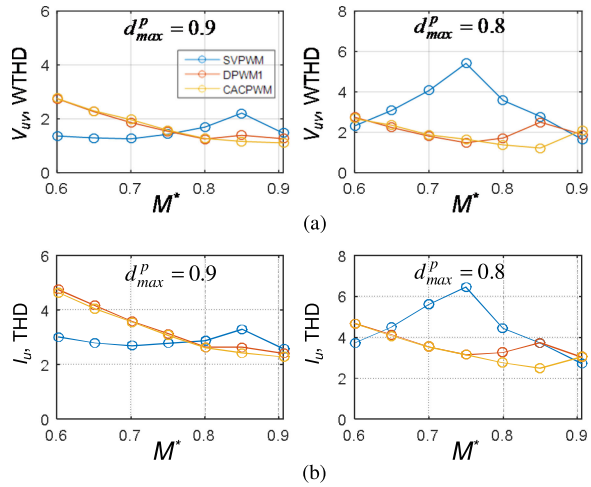

Fig. 22. Experimental results in the low current mode. (a) WTHD of V_{uv}. (b) THD of I_u.

clearly prove that the proposed CACPWM method has the best harmonic performance among all PWM methods.

VI. Conclusion

The deadtime and the bootstrap gate driver circuit mainly cause this duty ratio limitation in practice while resulting in the reduction of the linear modulation range of the VSI. To solve this problem, this paper proposed the new CACPWM method to restore the maximum linear modulation range of the VSI effectively. In addition, a linear compensation method is used for the deadtime compensation.

The performances of the proposed CACPWM method were evaluated by both simulation and experimental tests on the three-phase VSI system of 10 kW applied to the practical mild hybrid vehicle in the industry. Moreover, they were compared with those of the other existing PWM methods such as the space vector and discontinuous PWM methods. The result showed that the only the proposed method could restore the maximum linear modulation range of 0.906 for the VSI. Also, it could improve the harmonic performance effectively. For the further study, the overall PWM strategy including the over-modulation range is being investigated.

REFERENCES

[1] M. Lakka, E. Koutroulis, and A. Dollas, "Development of an FPGA-based SPWM generator for high switching frequency dc/ac inverters," *IEEE Trans. Power Electron.*, vol. 29, no. 1, pp. 356–365, Jan. 2014.

[2] A. M. Hava, R. J. Kerkman, and T. A. Lipo, "Carrier-based PWM-VSI overmodulation strategies: Analysis, comparison, and design," *IEEE Trans. Power Electron.*, vol. 13, no. 4, pp. 674–689, Jul. 1998.

[3] N. Mohan and T. M. Undeland, *Power Electronics: Converters, Applications, and Design*. New York, NY, USA: Wiley, 2007.

[4] R. K. Jardan, P. Stumpf, P. Bartal, Z. Varga, and I. Nagy, "A novel approach in studying the effects of subharmonics on ultrahigh-speed ac motor drives," *IEEE Trans. Ind. Electron.*, vol. 58, no. 4, pp. 1274–1281, Apr. 2011.

[5] Z. Ke, J. Zhang, and R. Raich, "Low-frequency current oscillation reduction for six-step operation of three-phase inverters," *IEEE Trans. Power Electron.*, vol. 32, no. 4, pp. 2948–2956, Apr. 2017.

[6] J. I. Itoh, G. T. Chiang, and K. Maki, "Beatless synchronous PWM control for high-frequency single-pulse operation in a matrix converter," *IEEE Trans. Power Electron.*, vol. 28, no. 3, pp. 1338–1347, Mar. 2013.

[7] O. Hui, Z. Kai, Z. Pengju, K. Yong, and X. Jian, "Repetitive compensation of fluctuating dc link voltage for railway traction drives," *IEEE Trans. Power Electron.*, vol. 26, no. 8, pp. 2160–2171, Aug. 2011.

[8] Y. Iwaji, T. Sukegawa, T. Okuyama, T. Ikimi, M. Shigyo, and M. Tobise, "A new PWM method to reduce beat phenomenon in large-capacity inverters with low switching frequency," *IEEE Trans. Ind. Appl.*, vol. 35, no. 3, pp. 606–612, May/Jun. 1999.

[9] Z. Hengbing, Q. M. J. Wu, and A. Kawamura, "An accurate approach of nonlinearity compensation for VSI inverter output voltage," *IEEE Trans. Power Electron.*, vol. 19, no. 4, pp. 1029–1035, Jul. 2004.

[10] T. Mannen and H. Fujita, "Dead-time compensation method based on current ripple estimation," *IEEE Trans. Power Electron.*, vol. 30, no. 7, pp. 4016–4024, Jul. 2015.

[11] Z. Zhendong and X. Longya, "Dead-time compensation of inverters considering snubber and parasitic capacitance," *IEEE Trans. Power Electron.*, vol. 29, no. 6, pp. 3179–3187, Jun. 2014.

[12] S. Yo-Chan, J. Ki Young, and S. Bum-Seok, "Integrated MOSFET inverter module for low-power drive system," *IEEE Trans. Ind. Appl.*, vol. 44, no. 3, pp. 878–886, May/Jun. 2008.

[13] R. M. Tallam and D. Leggate, "Control of a PWM voltage-source inverter in the pulse-dropping region to reduce reflected-wave motor overvoltage," *IEEE Trans. Ind. Appl.*, vol. 49, no. 2, pp. 873–879, Mar./Apr. 2013.

[14] R. J. Kerkman, D. Leggate, and G. L. Skibinski, "Interaction of drive modulation and cable parameters on ac motor transients," *IEEE Trans. Ind. Appl.*, vol. 33, no. 3, pp. 722–731, May/Jun. 1997.

[15] R. J. Kerkman, T. M. Rowan, D. Leggate, and B. J. Seibel, "Control of PWM voltage inverters in the pulse dropping region," *IEEE Ind. Appl. Mag.*, vol. 2, no. 5, pp. 24–31, Sep./Oct. 1996.

[16] Y. S. Lai and Y. K. Lin, "Quicken the pulse," *IEEE Ind. Appl. Mag.*, vol. 14, no. 5, pp. 34–44, Sep./Oct. 2008.

[17] J. T. Strydom, M. A. d. Rooij, and J. D. v. Wyk, "A comparison of fundamental gate-driver topologies for high frequency applications," in *Proc. 19th Annu. IEEE Appl. Power Electron. Conf. Expo.*, vol. 2, 2004, pp. 1045–1052.

[18] R. Mitova, J. C. Crebier, L. Aubard, and C. Schaeffer, "Fully integrated gate drive supply around power switches," *IEEE Trans. Power Electron.*, vol. 20, no. 3, pp. 650–659, May 2005.

[19] J. C. Crebier and N. Rouger, "Loss free gate driver unipolar power supply for high side power transistors," *IEEE Trans. Power Electron.*, vol. 23, no. 3, pp. 1565–1573, May 2008.

[20] A. Merello, "Bootstrap network analysis: Focusing on the integrated bootstrap functionality," Int. Rectifier Company, Appl. Note AN-1123, 2008.

[21] D. O. Neacsu, "Integrated circuits for power electronics applications," in *Proc. IEEE Int. Symp. Ind. Electron.*, 2010, pp. 4121–4169.

[22] V. Nguyen, J. C. Crebier, and P. O. Jeannin, "Compact, isolated and simple to implement gate driver using high frequency transformer," in *Proc. 26th Annu. IEEE Appl. Power Electron. Conf. Expo.*, 2011, pp. 1092–1098.

[23] P. Shihong and T. M. Jahns, "A self-boost charge pump topology for a gate drive high-side power supply," *IEEE Trans. Power Electron.*, vol. 20, no. 2, pp. 300–307, Mar. 2005.

[24] H. Fang, X. Feng, W. Song, X. Ge, and R. Ding, "Relationship between two-level space-vector pulse-width modulation and carrier-based pulsewidth modulation in the over-modulation region," *IET Power Electron.*, vol. 7, no. 1, pp. 189–199, 2014.

[25] J. Prieto, F. Barrero, M. J. Duran, S. Toral Marin, and M. A. Perales, "SVM procedure for n-phase VSI with low harmonic distortion in the overmodulation region," *IEEE Trans. Ind. Electron.*, vol. 61, no. 1, pp. 92–97, Jan. 2014.

[26] D. G. Holmes and T. A. Lipo, *Pulse Width Modulation for Power Converters: Principles and Practice*. Hoboken, NJ, USA: Wiley, 2003.

[27] E. R. C. da Silva, E. C. dos Santos, and C. B. Jacobina, "Pulsewidth modulation strategies," *IEEE Ind. Electron. Mag.*, vol. 5, no. 2, pp. 37–45, Jun. 2011.

[28] A. M. Hava, R. J. Kerkman, and T. A. Lipo, "Simple analytical and graphical methods for carrier-based PWM-VSI drives," *IEEE Trans. Power Electron.*, vol. 14, no. 1, pp. 49–61, Jan. 1999.

[29] A. M. Hava, R. J. Kerkman, and T. A. Lipo, "A high-performance generalized discontinuous PWM algorithm," *IEEE Trans. Ind. Appl.*, vol. 34, no. 5, pp. 1059–1071, Sep./Oct. 1998.

[30] B. Sun, I. Trintis, S. Munk-Nielsen, and J. M. Guerrero, "Effects and analysis of minimum pulse width limitation on adaptive dc voltage control of grid converters," in *Proc. IEEE Appl. Power Electron. Conf. Expo.*, 2016, pp. 1376–1380.

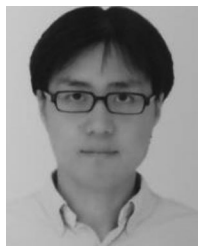

Jae-Goo Kim (M'18) received the B.S. and M.S. degrees in power electronics from Pusan National University, Busan, South Korea, in 2000 and 2002, respectively. He is currently working toward the Ph.D. degree at the School of Electrical and Electronic Engineering, Yonsei University, Seoul, South Korea.

Since 2002, he has been with Mando Corporation, Seongnam, South Korea, where he was a Senior Research Engineer to develop the inverter for electric power steering systems. He is currently a Team Leader to develop the motor drive system for hybrid and electric vehicles. His research interests include power conversion circuits and electric machine drives for automotive applications.

Kyo-Beum Lee (S'02–M'04–SM'10) received the B.S. and M.S. degrees in electrical and electronic engineering from Ajou University, Suwon, South Korea, in 1997 and 1999, respectively, and the Ph.D. degree in electrical engineering from Korea University, Seoul, South Korea, in 2003.

From 2003 to 2006, he was with the Institute of Energy Technology, Aalborg University, Aalborg, Denmark. From 2006 to 2007, he was with the Division of Electronics and Information Engineering, Chonbuk National University, Jeonju, South Korea. In 2007, he joined the Department of Electrical and Computer Engineering, Ajou University. His research interests include electric machine drives, renewable power generations, and electric vehicle applications.

Dr. Lee is an Associate Editor for the IEEE TRANSACTIONS ON POWER ELECTRONICS, the IEEE TRANSACTIONS ON INDUSTRIAL ELECTRONICS, the *Journal of Power Electronics*, and the *Journal of Electrical Engineering and Technology*.

Jung-Wook Park (S'00–M'03–SM'09) received the B.S. degree (*summa cum laude*) in power system and power electronics from Yonsei University, Seoul, Korea, in 1999, and the M.S.E.C.E. and Ph.D. degrees in power systems and power electronics from the School of Electrical and Computer Engineering, Georgia Institute of Technology, Atlanta, USA in 2000 and 2003, respectively.

He was a Post-Doctoral Research Associate with the Department of Electrical and Computer Engineering, University of Wisconsin, Madison, WI, USA, during 2003–2004, and a Senior Research Engineer with LG Electronics Inc., Seoul, South Korea, during 2004–2005. Since 2005, he has been with the School of Electrical and Electronic Engineering, Yonsei University, where he is currently a Professor. He is currently leading the National Leading Research Laboratory designated by the Korean Government to the subject of integrated optimal operation for smart grid. His current research interests include power system dynamics, energy management system, renewable energies based distributed generation system, operation and planning of microgrid, hardware implementation of power-electronic based inverters, etc.

Prof. Park was the recipient of Young Scientist Presidential Award in 2013 from the Korean Academy of Science and Technology, South Korea.